JOURNAL OF GEOPHYSICAL RESEARCH, VOL. 99, NO. D10, PAGES 20,829–20,845, OCTOBER 20, 1994

Response of an atmospheric general circulation model to radiative forcing of tropical clouds

Steven C. Sherwood,[1] V. Ramanathan,[1,2] Tim P. Barnett,[1] Mary K. Tyree,[1] and Erich Roeckner[3]

Abstract. The effects of upper tropospheric cloud radiative forcing (CRF) on the atmosphere have been examined using a recent version of the atmospheric general circulation model (AGCM) developed by the Max Planck Institute of Meteorology and the University of Hamburg. This model reproduces satellite-observed radiative forcing of clouds well overall, except that model maxima somewhat exceed those of observations. Three simulations have been performed where the clouds above 600 mbar have been rendered transparent to all radiation: first, throughout the tropics in the "NC" experiment; then only over oceans warmer than 25°C in the "NCW" experiment; and finally, only over the western Pacific warm oceans in the "NCWP" experiment. The local radiative effects of these clouds when they are present in the model are radiative heating of the middle to upper troposphere due to convergence of longwave and solar radiation; radiative cooling of the tropical atmosphere near and above the tropopause; a large reduction of solar radiation (50 to 100 W/m^2) reaching the surface; and a slight increase (5 to 20 W/m^2) in the downward longwave radiation at the surface. The removal of cloud radiative forcing significantly alters the circulation of the model atmosphere, as in previous AGCM studies, showing that a seemingly moderate heat source such as CRF is nonetheless capable of widespread influence over the global circulation and precipitation. The experiment responses include a significant weakening (in NCW) or rearrangement (in NCWP) of the Walker circulation. Zonal mean cloud cover, rainfall, and low-level convergence change modestly in the experiments, while zonal departures of these from their tropical means shift considerably. Regions over the warmest oceans which lose CRF become much less cloudy, indicating a positive local feedback to convection. The experiment circulation changes are diagnosed in terms of simple energy budget arguments, which suggest that the importance of CRF is enabled by the small magnitude of the atmospheric moist energy transport in the tropics. They also suggest that the response of the zonal mean atmosphere may be strongly dependent on the response of zonal eddies and on interactions between surface fluxes and tropospheric lapse rates. The response of the zonal eddies itself should be relatively independent of these interactions.

1. Introduction

The desire to predict climate change has spurred increasing efforts in recent years to develop and understand general circulation models of the atmosphere. While these models start with similar representations of the basic equations of fluid dynamics, they parameterize unresolved processes using a variety of strategies. The models, furthermore, exhibit widely varying responses to perturbations such as global warming scenarios. Recently, intercomparison studies have attributed the source of discrepancy to the parameterizations of clouds [*Cess et al.*, 1989]. A better understanding of cloud processes is needed to produce more reliable models of climate.

[1]Scripps Institution of Oceanography, University of California at San Diego, La Jolla.
[2]Also at Center for Clouds, Chemistry and Climate, Scripps Institution of Oceanography, La Jolla, California.
[3]Max-Planck-Institut für Meteorologie, Hamburg, Germany.

Paper number 94JD01632.
0148-0227/94/94JD-01632$05.00

Clouds and convection influence the Earth's climate by redistributing radiation and releasing latent heat. The latent heat release is a nonlocal transfer of heat from the oceans to the atmosphere, while the radiative effects, although perhaps smaller in absolute magnitude, are potentially more far-reaching since they can change the balance of the energy budget for the planet as a whole. In both respects the clouds tend to act as a time-varying, nonuniform heat source for the atmosphere and (usually) sink for the surface. The exact spatial dependence of this heating is poorly known, particularly in the vertical, and its statistics may depend significantly on a large variety of atmospheric parameters.

A number of simpler models of the tropical atmosphere and its response to heating precede this study, a notable early model being that of *Gill* [1980], who considered a linearized shallow-water equation model on a beta plane. The flow resulting from a tropical heat source off the equator included a pattern of ascent similar to that of the source and a zonally broad pattern of descent. *Hoskins and Karoly* [1981] developed a five-layer, spherical, baroclinic model linearized about the observed mean state. They found that subtropical heating would excite Rossby waves which

Table 1. Acronyms Used in This Paper

Acronym	Definition
CRF	cloud radiative forcing
SST	sea surface temperature
AGCM	atmospheric general circulation model
ECHAM3	current Hamburg version of the ECMWF (European Center for Medium-Range Weather Forecasting) GCM, used for all experiments in this study
WP	warm western Pacific area atmosphere (defined as a the area of SST > 25°C from 120°E to 180°E
APE	available potential energy
CAPE	convective available potential energy

readily propagate poleward, actually making subtropical forcing more efficient in exciting extratropical disturbances than forcing from higher latitudes. *Hartmann et al.* [1984] also analyzed the tropical circulation with a linearized primitive equation model with two different localized heating profiles. They found that a narrow heating profile centered at 400 mbar (representing the combined effect of condensation and the radiative heating which might result from a mature cloud cluster or "anvil," or, alternatively, from ice physics) produced a Walker circulation whose stream function more closely resembled observations than that resulting from a broader profile centered at 500 mbar (representing a classical heating profile resulting primarily from condensation).

Sardeshmukh and Hoskins [1985] examined the ECMWF-analyzed velocity and vorticity fields during the 1982–1983 El Nino Southern Oscillation (ENSO) event, finding that the response of the atmosphere to the measured heating anomalies displayed some important differences from those predicted by the linear models. For example, the observed vorticity budget was imbalanced in many southern hemispheric areas unless nonlinear terms were included in the equations. They also found asymmetric and low-frequency variability which they felt could not be simulated by a linear model. The importance of tropical upper level divergence in Community Climate Model 1 (CCM1) simulations of extratropical responses to sea surface temperature (SST) anomalies during the 1986 El Nino event was noted by *Hoerling et al.* [1992].

Numerous atmospheric general circulation model (AGCM) studies have examined the impact of cloud radiative forcing (CRF) (see Table 1) on the circulation [*Ramanathan et al.*, 1983; *Slingo and Slingo*, 1988; *Ramaswamy and Ramanathan*, 1989; *Randall et al.*, 1989]. See *Slingo and Slingo* [1988] for a detailed review of other previous efforts in this direction. The AGCM studies have generally shown that CRF strengthens precipitation and circulation patterns and have suggested that it must be parameterized accurately to simulate the tropical atmosphere. The present study is an attempt to continue the assessment of the radiative properties of clouds with a model whose treatment of cloud radiative properties compares favorably with observations and to understand further the mechanisms which are important in determining the nature of the atmospheric response to CRF. In particular, this study focuses on the middle to upper tropospheric clouds in the tropical region.

Our focus for this study stems from several recent developments. Satellite observations of CRF [*Harrison et al.*, 1990] revealed that the tropical regions are subject to large monthly mean values, 50 to 100 W/m^2, of longwave and shortwave cloud forcing. Radiation model calculations [e.g., *Stephens and Webster*, 1979] indicate that optically thick clouds within the middle to upper troposphere are required to account for longwave cloud forcing in excess of 50 W/m^2. The peak values of 100 W/m^2 occur over warm oceanic regions of the tropical western Pacific, Atlantic, and Indian Oceans, which are centers of deep convection. Large-scale circulation is inextricably involved in this system of convective and extended, upper tropospheric cloudiness. First, it provides a source of moisture for deep convection through low-level convergence. Second, it is driven mainly by the latent heat released in deep convection and by the longwave and shortwave cloud forcing [e.g., *Houze*, 1982]. To gain a quantitative understanding of this complex feedback, it is necessary to ascertain the relative importance of the individual components. We single out tropical CRF in this study primarily because its role as a source of diabatic forcing for the general circulation is poorly understood.

We begin by describing the model in section 2. Section 3 compares the control atmosphere to available observations. Section 4 describes the experiment and section 5 the results. Section 6 discusses the results and gives some interpretations.

2. Model Description

The AGCM used in this study was developed by the modeling group at the Max Planck Institute at Hamburg and University of Hamburg. The model adopts the dynamical framework of the European Center for Medium-Range Weather Forecasting (ECMWF) model, but incorporates treatments of physical processes developed at Hamburg, and is referred to as ECHAM (for ECMWF-Hamburg). The particular version of the model used here is the most recent version of the model at the time of this study (ECHAM3) which incorporates the following physical processes: (1) penetrative convection scheme of *Tiedtke* [1989], (2) transport of water vapor and cloud water, (3) fractional cloudiness scheme, (4) dependence of cloud optical properties on model cloud water, (5) a diurnal cycle, (6) boundary layer processes, and (7) surface energy transfer processes for computing land surface transfer.

The control version of the model has been run for 10 years from 1979 to 1989 with observed SSTs and seasonally and diurnally varying solar insolation. A detailed model description and basic climatology can be found in the work of *Roeckner et al.* [1992]. Since the detailed simulations have not been widely published, we include a model validation here, focusing only on those aspects that are relevant to this study.

3. Model Validation

To gain some confidence in the present model's ability to provide realistic radiative heating profiles, in the sections below we assess the ability of the model to simulate actual humidity distributions in the tropics and its ability to predict longwave and shortwave cloud forcing quantitatively.

3.1. Comparison With Radiosonde Data

To estimate the success of the model in predicting vertical humidity and cloud distributions, we compare an ensemble

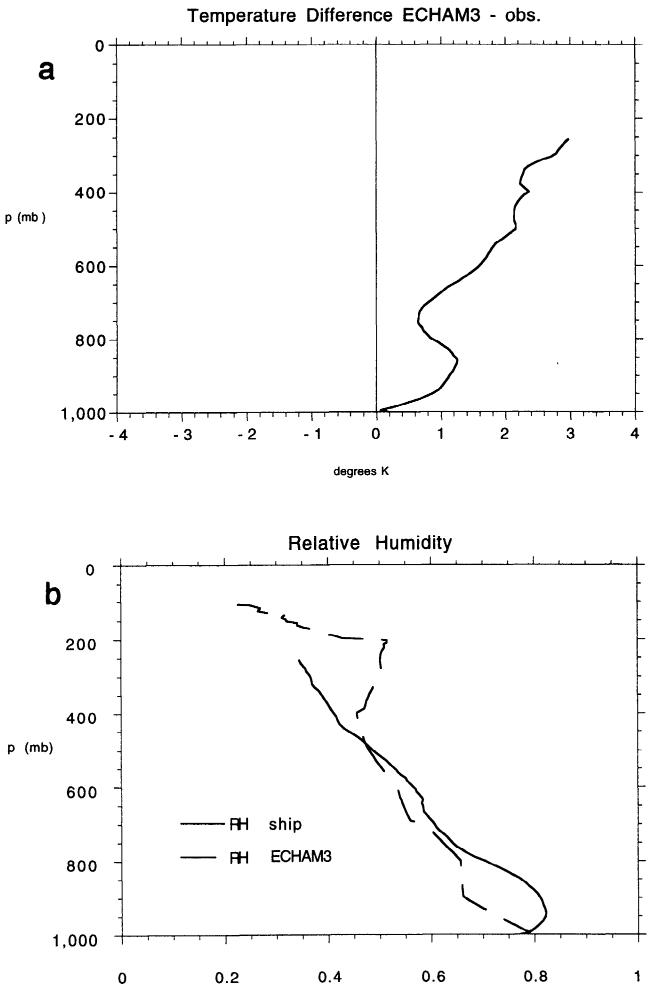

Figure 1. Mean warm pool atmosphere (a) temperature difference, ECHAM3 (ECMWF-Hamburg) and ship, and (b) relative humidity, from ship observations and ECHAM3. Ship observations are from the National Center for Atmospheric Research upper air data set from 1985 to 1989 within the region 130°E to 160°E and 20°S to 20°N. The ECHAM3 averages were computed from spatially and temporally co-located 1985–1989 control run values.

of model soundings with the National Center for Atmospheric Research upper air data set from the years 1985 through 1988. These data include 182 soundings launched from ships at 0000 UT in the region bounded by 130°E to 160°E longitude and 20°N to 20°S latitude, a region of frequent deep convection. A matched set of soundings was obtained from the ECHAM3 simulations, where each ship sounding was matched to the nearest model grid point and the nearest biweekly time (1st or 15th of each month). The averages of each ensemble of soundings appears in Figure 1, with the temperatures plotted as a difference. The model produces a moderate warm bias in this region, which peaks at about 2°C near 300 mbar. There is also a moist bias above 500 mbar (although the accuracy of sonde humidities above 500 mbar is questionable) and a dry bias below which decreases to zero at the surface. Similar discrepancies were noted by *Tiedtke* [1989] in comparisons between a one-dimensional model incorporating his cumulus parameterization and Global Atlantic Tropical Experiment data. He attributed the discrepancy to overestimation of deep convection behind the ridge of a tropical wave disturbance, at the expense of shallow convection. Thus there is a possibility that ECHAM3 will overestimate high cloud and underestimate low cloud to some degree.

3.2. Comparison With Earth Radiation Budget Experiment (ERBE) Cloud Forcing Measurements

Satellite observations provide a more direct test of the ECHAM3 accuracy in handling cloud and atmospheric radiation. We have examined the cloud shortwave forcing, longwave forcing, and total and atmospheric greenhouse effects of the model for April 1987 for comparison with the ERBE observations of *Ramanathan and Collins* [1991], mimicking their Figure 2 with ECHAM3 equivalents. Their results and ours are shown together in Figure 2.

We briefly describe the observed fields in this figure. The total greenhouse effect, G, is the reduction in the top-of-atmosphere outgoing longwave radiation (OLR) by clouds and the atmosphere, compared to that emitted at the surface. It is divided here into two components, $G = Ga + Cl$, where Ga is the reduction in OLR by the clear atmosphere and Cl, the total cloud longwave forcing, is the reduction due to clouds and cloudy atmosphere. The total shortwave cloud forcing, here Cs, is similarly defined as the difference between the observed cloudy and the clear-sky albedos at a given location. *Ramanathan and Collins* [1991] assert that the sharp increase in G above SSTs of 300 K is due to a sharp increase in the frequency of deep convection in oceanic regions at these SSTs. However, they note that the increase in G is not due to the convective clouds themselves but rather to the extended middle to upper tropospheric clouds resulting from the convection, since the horizontal extent of these anvils greatly exceeds that of the convective clouds. The ECHAM3 is able to capture this important feature. The slope of Ga with SST becomes steeper when SST exceeds the convection threshold of 300 K because of the moistening of the upper troposphere associated with convection and the change in lapse rate [*Hallberg and Inamdar*, 1993]; again the model is able to capture these changes. Finally, the scatterplot of shortwave and longwave cloud forcing reveals that the clouds that trap significant longwave radiation also reflect comparable solar energy back to space. This near cancelation of longwave and shortwave cloud forcing is a characteristic feature of extended clouds over warm oceans.

The scatterplot of model atmospheric greenhouse effect (Figure 2a–2c) shows good agreement with the ERBE observations, suggesting that the model is simulating correctly the forced large-scale circulation, the water vapor distribution, and the longwave absorption of the vapor. The total greenhouse effect simulation is also good, vindicating the model's cloud radiative forcing and atmospheric response to SST. The exaggeration of the greenhouse effect at very high SSTs is probably due to the absence of atmosphere-ocean feedbacks which is an unavoidable consequence of prescribing the SST [*Waliser et al.*, 1993]. Finally the Cl versus Cs plot shows magnitudes and correlation similar to those of ERBE, except for a spreading of the cloudier cases out to maxima greater than the maxima seen by ERBE, which could also be due to lack of an interactive ocean. While the increase in maximum forcing may again indicate an overestimate of high cloud, the agreement in apparent slope between the model and the observations indicates that cloud radiation physics in the longwave and shortwave are being modeled consistently,

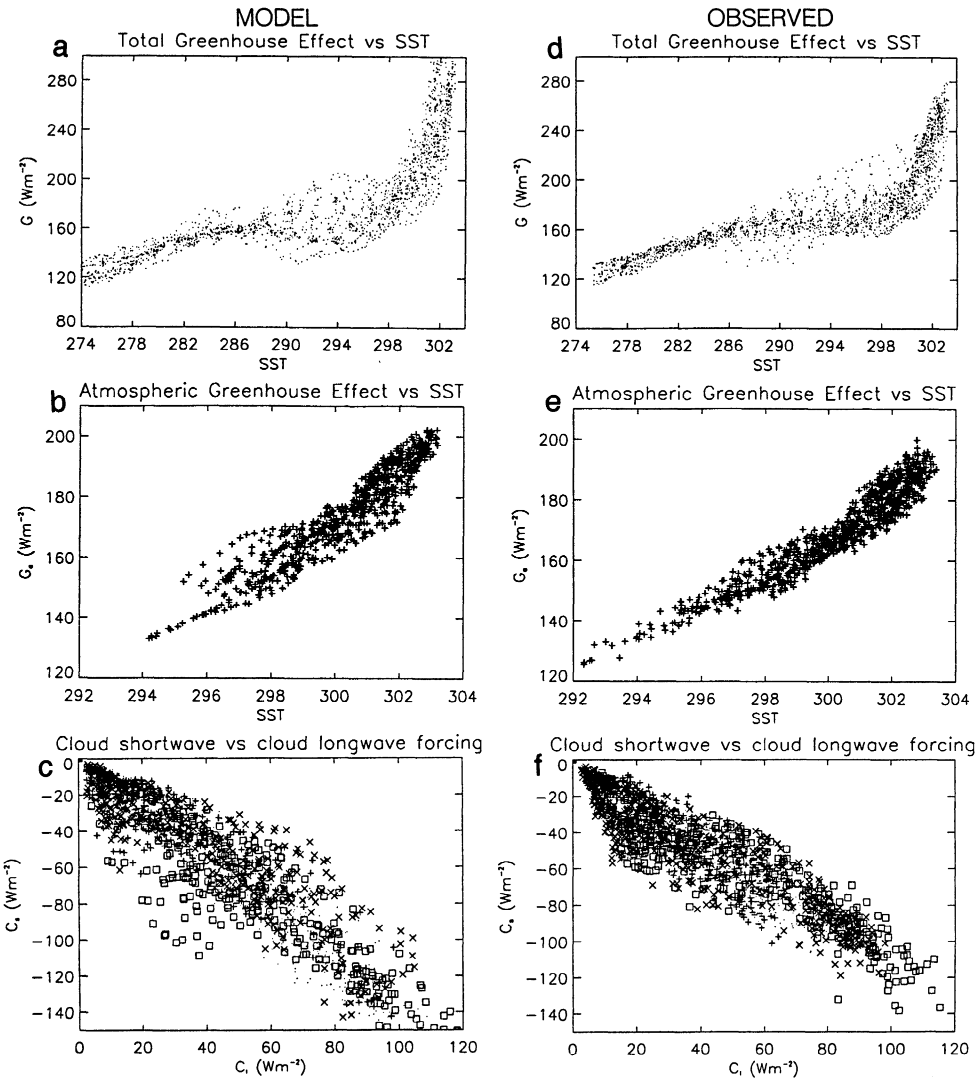

Figure 2. (a) Earth Radiation Budget Experiment (ERBE) monthly mean total greenhouse effect plotted against sea surface temperature (SST), April 1987, reported by *Ramanathan and Collins* [1991]. (b) ERBE atmospheric greenhouse effect against SST for the tropical Pacific, April 1987. (c) ERBE cloud shortwave forcing against cloud longwave forcing, 10°N to 10°S, 4/85, 2/87, 2/88, 4/87. (d)–(f) as in Figures 2a–2c except ECHAM3 simulations.

a luxury which is by no means to be taken for granted in an AGCM but which is extremely important for the generation of realistic net heating profiles [*Ramaswamy and Ramanathan*, 1989; *Stephens and Webster*, 1979].

Although these diagnostics may not necessarily reveal all potential model shortcomings, they reassure us that the ECHAM3 model can adequately reproduce the net radiative heating due to both the cloud cover itself and the fluctuations in the atmosphere in which the clouds are embedded.

4. Design and Description of the Sensitivity Experiments

To explain the rationale behind the design of the experiment, we provide a brief description of how clouds influence the atmospheric radiative heating profile and the peculiarities of the tropical atmosphere.

The satellite data in Figure 2 illustrates the net radiative effects of clouds on the surface-atmosphere column. This by itself is an inadequate description of their effects since the vertical distribution of the heating profile is critical. For example, over the tropical Pacific warm pool, the longwave and shortwave cloud forcings nearly cancel one another, such that the net effect is very small. Does this mean that clouds have no net effect on the tropical atmosphere? No, because the vertical distributions of the shortwave and longwave heating are quite different. The shortwave effect of clouds is mostly to reduce the solar heating of the surface, but they also cause a slight cooling of the atmosphere below the cloud (due to reduction of shortwave heating) and a slight warming at cloud top due to absorption. Clouds absorb longwave radiation from the surface which tends to heat their bases. They also emit longwave upward and downward, which tends to cool the cloud top and base. In general, for optically thick clouds the base is subject to a net longwave heating (since absorption of surface radiation exceeds emission) and the top is subject to a net cooling because of emission to space. Also, the clear atmosphere below the cloud is heated by the enhanced downward radiation from cloud base. This heating, even if it is from high-altitude cirrus, can extend through most of the troposphere below (unless it is intercepted by lower clouds) since most of the clear-sky absorption occurs in the lower troposphere where water vapor is abundant.

The longwave effect of clouds depends strongly on the altitude of clouds. As cloud altitudes increase, the cloud top cooling decreases, so that the net effect can switch from net cooling for low clouds to net heating for high clouds. High surface temperatures cause the tropical upper tropospheric clouds to have an extreme effect for two reasons. First, the surface emission is large, which maximizes the cloud base heating. Second, the high surface temperatures cause deeper convection, penetrating to altitudes of 15 to 18 km. The resulting anvils are cold and the cloud top emission is reduced significantly. As a result, clouds in the upper troposphere can be subject to a large net longwave heating. This heating effect is enhanced by absorption of solar radiation by ice crystals.

The net effect in the tropics is one of a diabatic dipole: radiative heating of the entire troposphere with maxima in the cirrus layers (8 to 15 km) and a comparably large cooling of the surface. The qualitative pattern is similar to moist thermodynamics, that is, evaporative cooling of the surface and latent heating of the troposphere.

To illustrate the effects of upper tropospheric clouds, we perform a control simulation, and then a series of three experiments in which the cloud radiative effects are removed over successively more restricted areas of the tropics. Since our fundamental motivation is to examine the importance of the extended cloudiness resulting from convection, in our experiments we systematically delete the radiative effects of clouds above 600 mbar. Our goal is not only to gauge the gross global radiative effect of high cloud but also to gain some insight into the local and nonlocal mechanisms by which cloud radiative heating influences the global climate. The three experiments and their modifications to the radiation parameterization are (1) NC (no cloud radiative forcing): all clouds above 600 mbar and located between 25°N and 25°S are rendered transparent to both longwave and shortwave radiation; this includes clouds over land; (2) NCW (no cloud radiative forcing over warm water): clouds above 600 mbar and located over ocean warmer than 25°C are rendered transparent; those over land and cooler ocean are unaffected; and (3) NCWP (no cloud radiative forcing over the western Pacific): same as NCW except that only clouds between 120°E and 180°E longitude are made transparent; the affected region will be designated "WP" hereafter.

Each simulation, including control, was integrated from March 1 to August 31, 1985. The experiments were initialized using the control atmospheric state from the previous day; that is, the cloud radiative interactions were removed starting on March 1. The time series of mean 200 mbar temperature within 25° of the equator in the NCW run, taken as an index of model response to the perturbation, decayed roughly exponentially from initialization to a new steady value with a time constant of about 30 days. The NCWP and control runs were repeated for July only, with a complete set of diagnostics added to yield vertical profiles of heating and moistening due to all causes, or "tendencies." These repeat runs will therefore be referred to as tendency runs, and the tendencies will be used to help interpret the experiment response. They will not be exactly the same as those occurring in the full summer simulations (which are not available).

All figures in section 5 of this paper are from the June, July, and August averages of the initial runs, unless otherwise indicated. The figures in section 6 are from the tendency runs. The main conclusions of this study do not rest on the significance of small or highly localized experimental responses, so to check significance, we have simply compared important experiment responses in the summer averages with those in the May portion of the initial runs and in the tendency runs. All responses discussed in the text (e.g., changes to the area average of a model variable) did not differ among members of this ensemble by more than 5% of the control value. Any temperature change above the boundary layer was reproduced to accuracy at least 20% of the change itself.

As noted in previous AGCM studies [*Slingo and Slingo*, 1988, hereinafter referred to as SS; *Randall et al.*, 1989, hereinafter referred to as RHDC], it is important to distinguish the direct effects of CRF from the indirect effects. The loss of this important source of atmospheric heating modifies the circulation, which in turn modifies the distribution of water vapor and the formation of clouds, including the latent heat release which this produces. The change in clear-sky radiative heating and the change in latent heating will each then produce indirect changes to the circulation in addition to those caused by the cloud forcing itself. Another important point is that only the atmospheric heating portion of CRF has been removed in our experiments; the ocean cooling has implicitly been left in place, since the observed SSTs (which are influenced by real-world solar radiation) are unchanged in the experiments.

The one exception to this is that surface shortwave changes occur in the NC run over land and have a warming effect in this experiment. ECHAM3 does not fix land temperatures as with SST but predicts them using a five-layer soil model. Diurnal fluctuations in land temperatures, for example, are of critical importance to land weather and its influence on the global circulation. We have included NC to provide a comparison with the results of previous studies and to see how much difference CRF over land makes. However, we feel that increasing surface heating over land confuses the issues that we are attempting to address and will concentrate our attention on the other runs. Our NCW experiment is an attempt to remove the effect of land heating without removing the land, since realistic geography is necessary to assess the impact of CRF on any actual features of the Earth's circulation such as the Walker cell. Our strategy will still cause some unnatural atmospheric contrasts at some of the coasts due to the abrupt change in radiative heating. Some of the strongest modifications to circulation on small scales occur near land-ocean boundaries, although this is also true of the NC simulation.

Both the SS and RHDC studies and many observational studies [e.g., *Johnson et al.*, 1987] establish the warm pool region of the western Pacific as perhaps the Earth's most significant region of atmospheric diabatic heating. The NCWP experiment is designed to see how important the CRF in the warm pool is relative to that over the rest of the tropics. This experiment will also show more clearly than NCW how the atmosphere responds to localized heating anomalies.

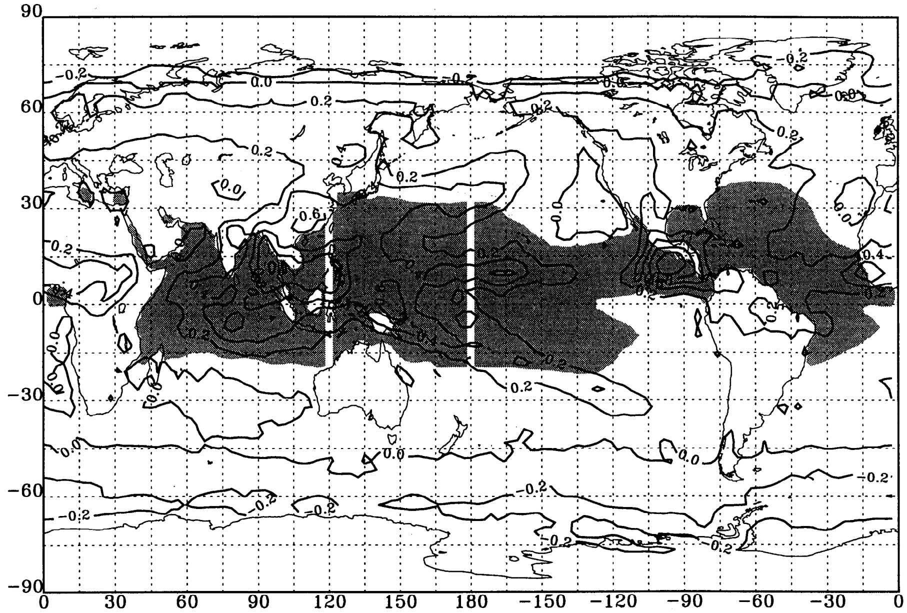

Figure 3. Tropospheric average atmospheric cloud radiative forcing in the control run; contour interval is 0.2°C/d. The shaded region indicates areas whose SST exceeded 25°C at least half the days during June–August, showing the approximate area where cloud radiative forcing (CRF) was eliminated in the NCW (no cloud, warm water) experiment. In the NCWP (no cloud, western Pacific) experiment, only the CRF in the shaded region between the two white lines was eliminated.

5. Experiment Results

5.1. Control Run Heating

The air at a fixed location in the atmosphere may be heated by means of advection, diffusion, and diabatic energy release. In the tropics the advection of energy is dominated by vertical motions (time- and column-averaged atmospheric advection by horizontal motions in the western Pacific atmosphere is smaller by a factor of 9). The vertical advection or "adiabatic cooling," $w\ \partial\theta/\partial z$, is a strong cooling term in tropical regions of ascent since the lapse rate is significantly subadiabatic. Diffusion in the model includes eddy diffusion, which is significant only in the lowest layers, and mixing caused by deep, midlevel, and shallow convection. The diabatic heat sources are radiative heating and cooling, latent heat release through condensation of water vapor, and latent cooling by reevaporation of condensed water. ECHAM3 generates latent heating both in parameterized cumulus convection and in saturated regions in the absence of parameterized cumulus (this is called "large-scale condensation").

Figure 3 shows the geographical distribution of CRF. This distribution is highly nonuniform. The vast majority of the tropical cloud forcing and associated latent heating is concentrated in the warm pool and Asia, but cloud is also generated over Central America and Africa. The high cloud over Central America is part of a monsoon circulation generated by the model in this area which significantly exceeds observations. We will not discuss the behavior of this feature in the experiments except as part of the overall equatorial response.

Also shown in Figure 3 is the region, SST > 25°C, over which the CRF was removed in the experiments. The two white lines indicate the region affected in NCWP (the "WP" region), while the entire shaded region is affected in NCW. The region shown covers model locations whose SST met the threshold at least half the days (the excursion of the 25°C isotherm during the summer was no more than a few degrees latitude). The vertical structure of WP region heating from the July tendency run appears in Figure 4, along with the heating profiles due to cumulus convection (CV) and large-scale condensation (LH).

5.2. Cloud Radiative Forcing (CRF) Effects on Temperature and Zonal Jets

As in previous model studies, the cloud radiative forcing in the current experiment causes heating in most of the middle and upper tropical troposphere, both in the form of longwave convergence below cirrus anvils and in the shortwave absorption within anvils. The loss of this heating in the experiments caused the temperature to drop throughout the

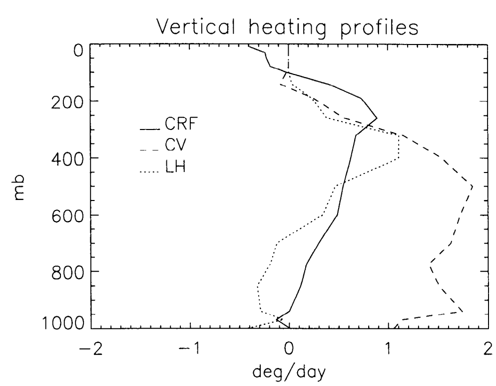

Figure 4. Western Pacific (WP) region average vertical heating profiles due to CRF; cumulus convection, including mixing and net latent heat release (CV); and large-scale (any nonconvective) net latent heat release (LH); units are °C/d.

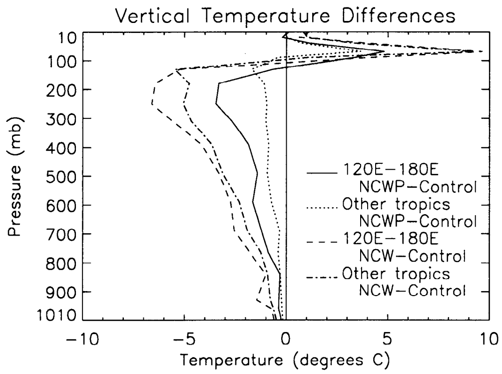

Figure 5. Vertical profile of temperature change between the experiment and the control runs. Solid lines, WP area (120°E–180°E, SST > 25°C), NCW, and NCWP; dotted lines, other tropics, 25°N–25°S, land excluded.

troposphere but increase in the lower stratosphere, as shown in Figure 5 where the temperature changes are shown both for the WP region and for all tropics. The reasons for stratospheric warming are not definite, but loss of cloud top cooling accounted for at least some of it. Tropical temperatures are well known to be nearly uniform in the free troposphere, and the longitudinal variation of the temperature change there (not shown) was also quite uniform except for a moderate increase over the WP area. The vertical distribution of the temperature change matched that of the cloud forcing, increasing with height and becoming negative above the tropopause. While the NCW experiment showed an average cooling of about 7°C over the WP region at 200 mbar, the NCWP run showed only about half this cooling even within the WP region and less than 1°C cooling outside.

The control and experiment runs of the model generated strong subtropical westerly jets in the upper tropospheres of each hemisphere, as observed. These jets are in geostrophic balance with the meridional temperature gradients, increasing with altitude throughout the lower and midtroposphere, where the equatorial atmosphere is warmer than the extratropical air due to the increased diabatic heating, and then abruptly decreasing between the 200-mbar level and the tropopause at 100 mbar, where the meridional gradients are reversed due to tropical cooling. The temperature adjustments in the tropics during the experiments were reflected in a general weakening of these subtropical jets.

5.3. CRF Effect on General Circulation

The western Pacific is a region of large-scale atmospheric ascent. This ascent is associated with net radiative and condensational heating in the area, which is then carried to midlatitudes by the Hadley cells (by which we refer here to the zonally averaged, large-scale meridional tropical and midlatitude circulations) and to the eastern Pacific by the Walker circulation (a zonal circulation with ascent in the western Pacific and descent in the eastern Pacific). These circulations respond to the available potential energy (APE) generated by the heating [*Lorenz*, 1955]. A map of the control summer velocity potential at 200 mbar appears in Figure 6. The velocity potential χ is related to the horizontal divergence δ of fluid in the model layer by

$$\delta = \nabla^2 \chi$$

so that the velocity potential is a smooth field with the same general properties. Divergence (negative velocity potential) at 200 mbar is associated with large-scale, deep ascent. Figure 6 shows a very broad pattern of ascent over the western Pacific past the date line and including eastern Asia. Air was descending over most of the southern hemisphere, particularly southern Africa. The zonal gradients in χ appear somewhat stronger than the meridional gradients, indicating that zonal circulations were at least as strong as meridional ones, even at the peak of the seasonal cycle.

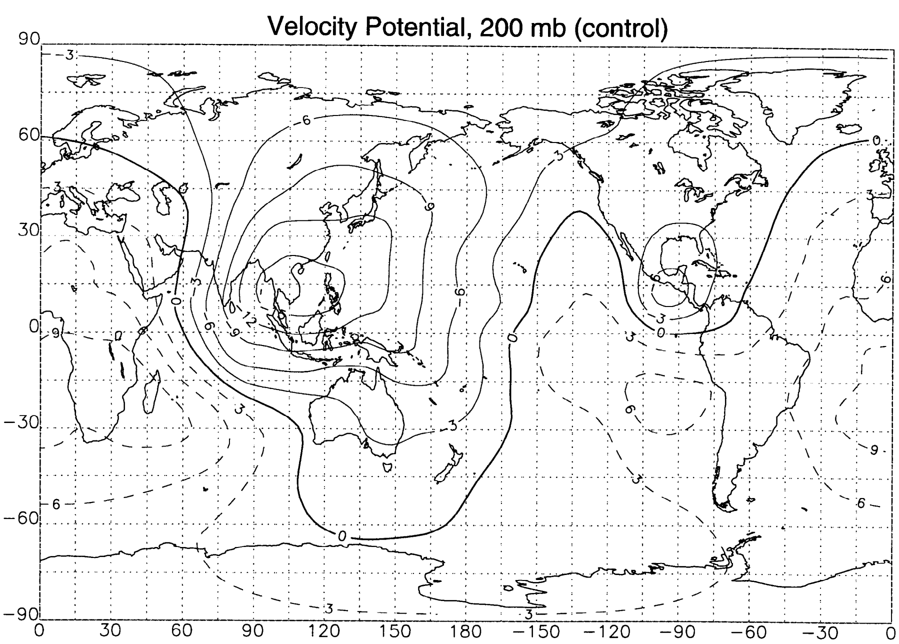

Figure 6. Velocity potential at 200 mbar from the control run; contour interval is 3.0°E^6 m^{2}s^{-1}. Zero contour is thick; dashed contours are positive.

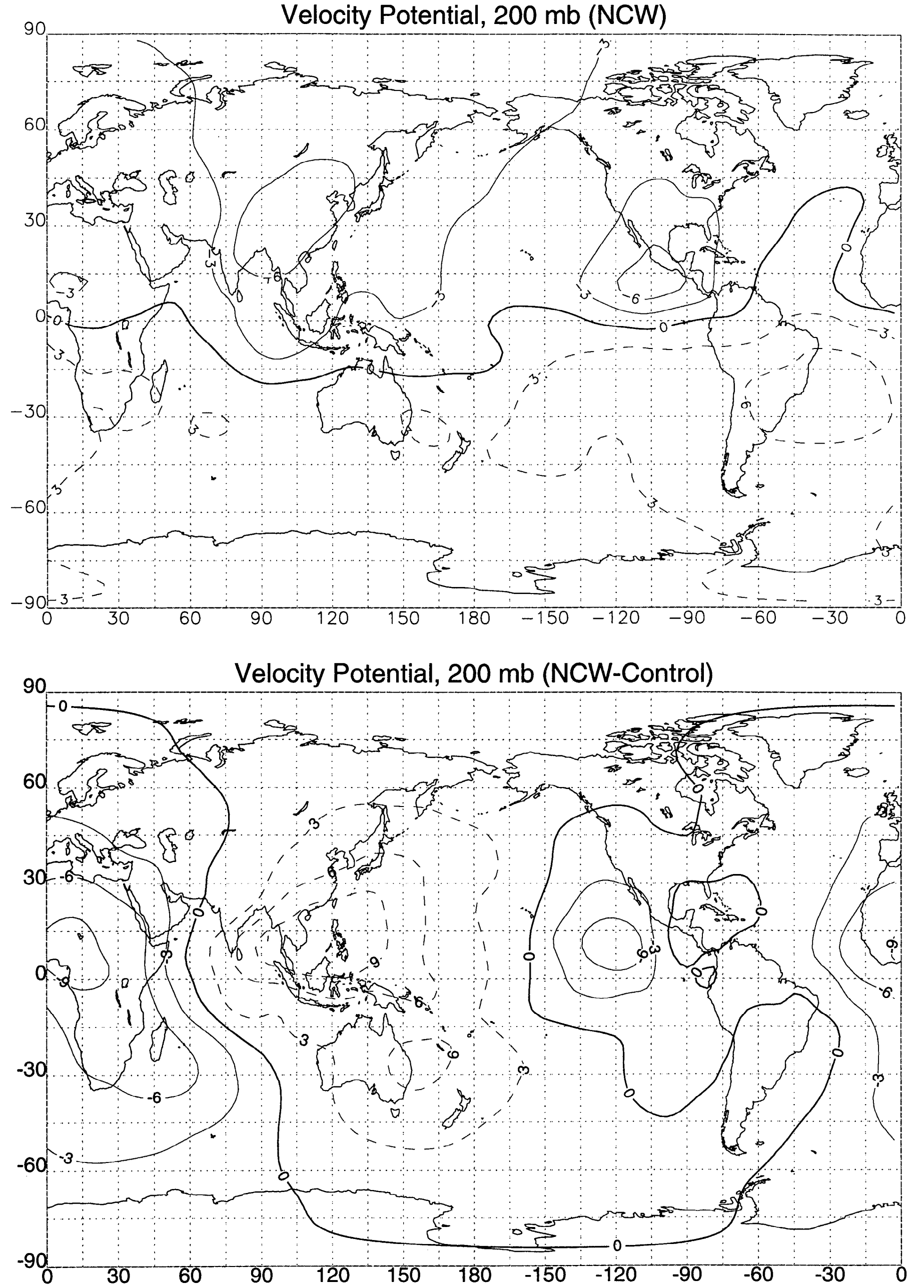

Figure 7. (a) As in Figure 6 except NCW run. (b) Difference between Figures 7 and 6; contouring is identical to Figure 7a.

This was no longer true in the NCW simulation, where zonal circulations weakened considerably (Figure 7a). Comparison of Figures 7b and 8b shows that an anti-Walker type zonal circulation anomaly developed in both experiments. This anomaly was stronger in NCWP (where only the WP region lost CRF) than in NCW, but for both experiments its magnitude was of the same order as that of the zonal circulation itself (Figure 6).

The (zonally averaged) Hadley response was more modest. Figure 9 shows the vertical velocity at 500 mbar versus latitude. The Hadley circulation weakened more in the NCW simulation than NCWP, with ascent from the equator to 20°N dropping by about 25%, compared with about 10% for NCWP (examination of lower and upper tropospheric divergence maps, not shown, leads to similar conclusions). There was about a factor of 3 increase in lost tropical cloud heating between the NCW run and the NCWP run, which roughly matches the ratio of the changes in ascent. Another change occurring in the meridional circulations of both experiments was that the winter Hadley subsidence moved farther south. This was associated with the appearance of a narrow convection band just north of Australia which did not exist in the control run (see Figure 10). Thus a fairly strong meridional eddy anomaly appeared in both experiments within the WP region of perhaps 20° latitudinal extent, which accounts for much of the 10 and 25% zonal average figures.

Figure 11 shows the vertical variation of vertical velocity in the WP region in the control and NCWP experiments. These profiles show that the control WP divergence varies monotonically with height to at least 200 mbar and recon-

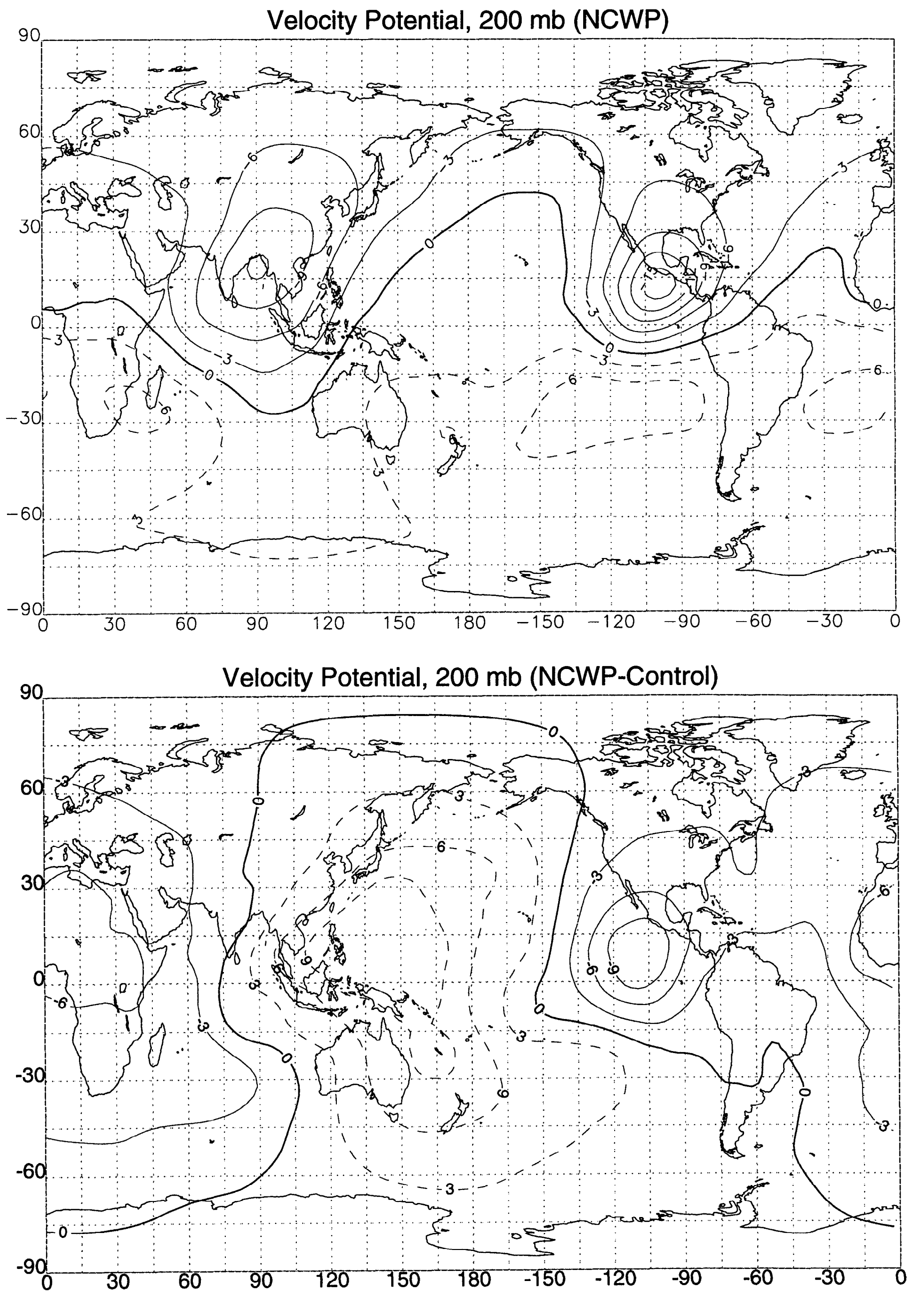

Figure 8. (a) As in Figure 6 except NCWP run. (b) Difference between Figures 8a and 6; contouring is identical to Figure 8a.

firms that the experiment circulation changed acutely in the upper atmosphere. The horizontal distributions look quite similar at different altitudes, so we take the 500-mbar velocity to be a reasonable indicator of overturning mass flux at least within the Hadley and Walker cell domains. We also examined the distribution of χ at 850 and 900 mbar (not shown), which was nearly a mirror image of the 200-mbar pattern, as expected.

5.4. Effect on Tropical Deep Convection and Cloudiness

Does the loss of cloud radiative heating cause more or less high cloud to form as a response? This question is equivalent to asking whether clouds provide a positive or negative feedback to convection through their radiative effects on the atmosphere. On the one hand, we have seen that cloud radiative heating increases local large-scale ascent and low-level convergence. This should promote the formation of more clouds of all types in the region of heating. On the other hand, the heating occurs above the boundary layer which tends to increase the stability of the atmosphere, reducing the convective available potential energy (CAPE) which measures the energy available for localized deep convection. This should suppress deep convection.

The geographical and vertical distributions of total cloudiness in each run are shown in Figure 12. The model cloudiness decreased in most areas which lost CRF, where the vertical distributions of cloudiness indicate a substantial loss of cloud in the midtroposphere and a thinning of cirrus anvils (the peak from 100 to 300 mbar). In particular, the NCWP simulation produced only about half the cloudiness

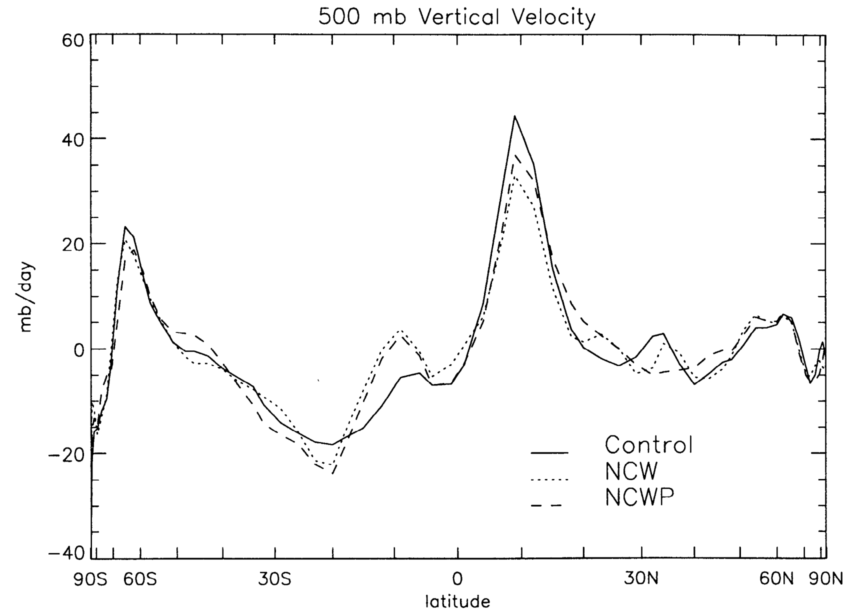

Figure 9. Zonal average 500 mbar vertical velocity (in mbar/d), defined positive upward, against latitude: control (solid line), NCWP (dashed line), NCW (dotted line).

in the WP region at most altitudes. However, lost cloudiness over the WP was made up by increases in other ocean and land areas. In the NCW run, losses were much bigger over Indonesia and no compensating gains occurred in the Indian Ocean, but gains occurred more strongly over land. There was also some gain over the eastern Pacific and Atlantic Oceans even though CRF was lost there; we speculate that this was because, over these oceans the model's stability condition for convection was usually met in NCW but not in the control run, while over the warmer oceans it was already met most of the time in the control run. In summary, the cloudiness was zonally redistributed away from areas losing CRF and toward the colder oceans, but the net overall tropical cloudiness change was not large in either experiment despite the broad upper tropospheric cooling and overall gain in CAPE (our CAPE calculations follow *Williams and Renno* [1993] except that we employ 50% latent heat of fusion, midway between their "ice" and "no ice" irreversible cases) (see Tables 2a and 2b).

The increase in CAPE does seem to have been responsible, however, for an overall loss in low cloud in the experiments, particularly NCW. Higher CAPE in this experiment

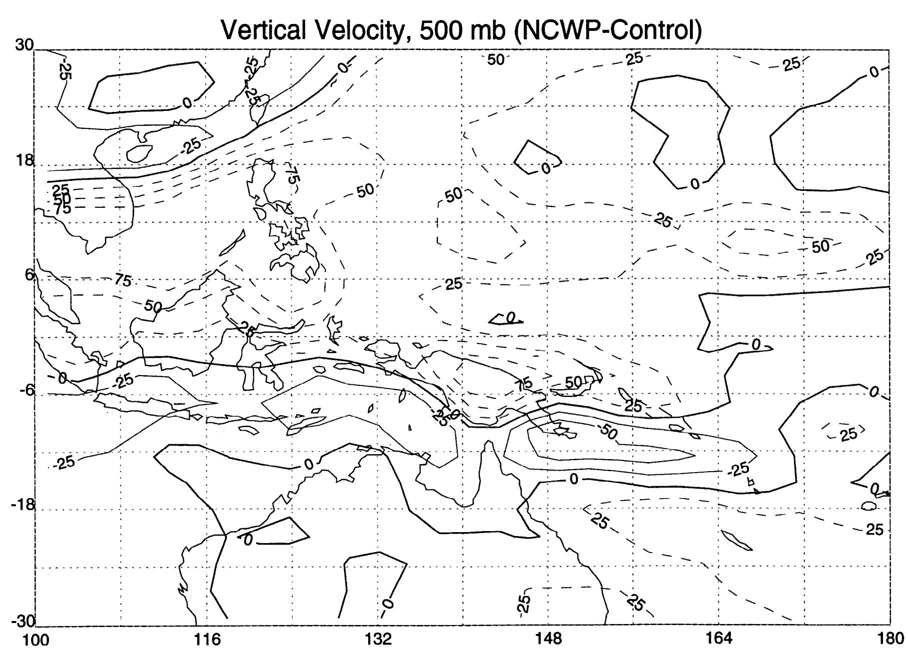

Figure 10. Map of 500 mbar vertical velocity difference, NCWP - control, over the Pacific Ocean. Contour interval is 25 mbar/d. Thick contour is zero; dashed contours are negative (indicating more downward motion in NCWP).

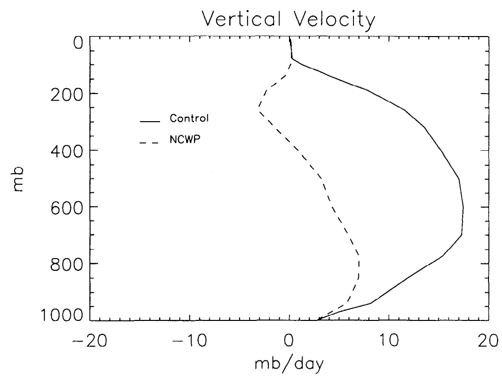

Figure 11. Vertical profile of mean vertical velocity in the WP region in mbar/d, defined positive upward, from the control and NCWP tendency runs.

resulting from the upper tropospheric cooling caused convection to be deeper and nearly all condensation over tropical oceans to be convective. The sharp reduction in low-cloud formation means that the exclusion of low-cloud CRF from removal in our experiments probably made little difference, since evidently (in the model) these clouds depend partly on high-cloud heating for their existence. Furthermore, low clouds have small column-averaged atmospheric CRF, which can become even smaller if they overlap with higher clouds, since the latter determine the emission to space if they are optically thick. ECHAM3 assumes maximum cloud overlap in convective areas between adjacent, cloudy model levels.

The regional changes in total latent heating (precipitation) resemble those of cloudiness but are more subtle. Figure 13 shows the longitudinal variation averaged between 20°S and

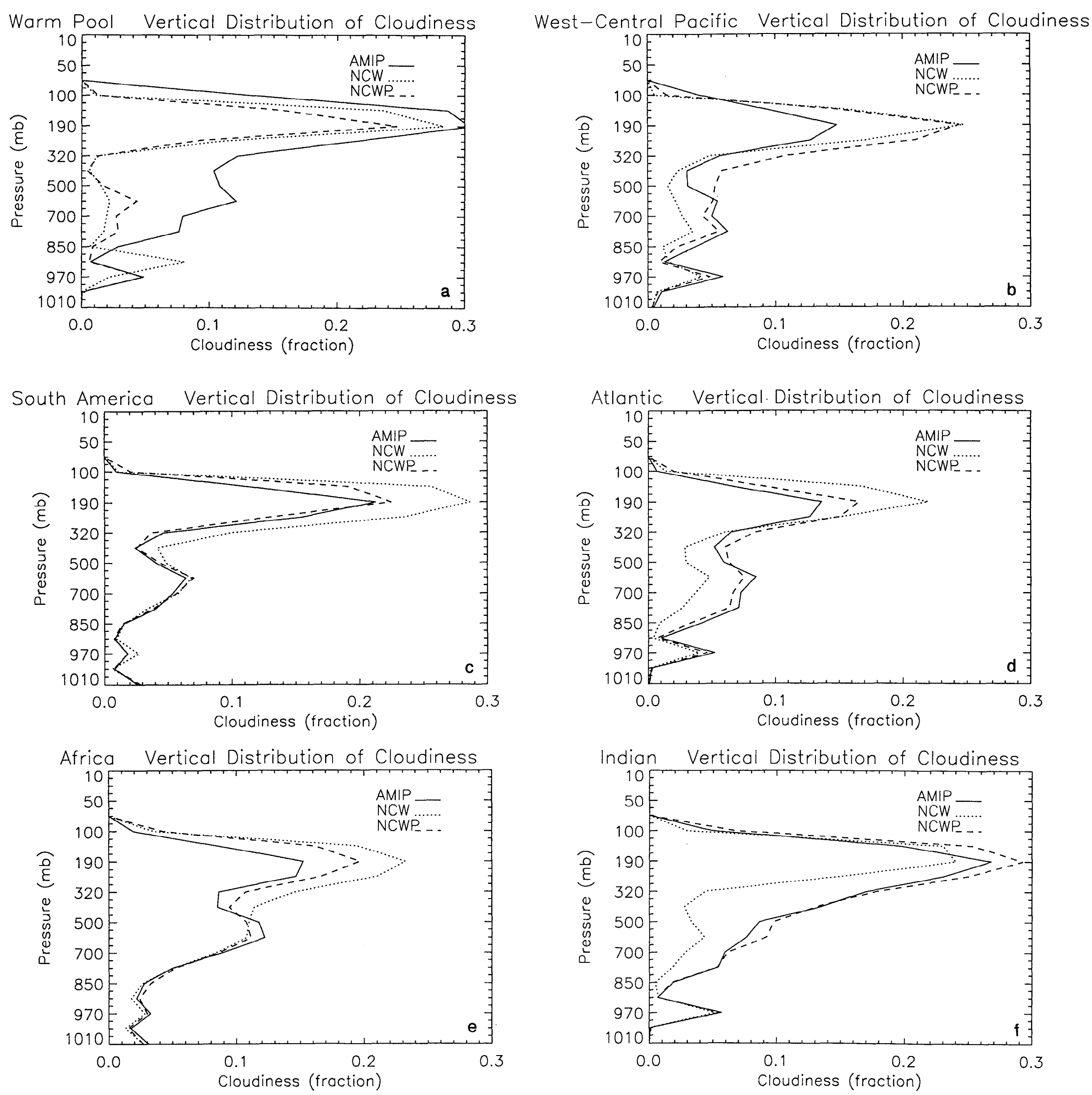

Figure 12. Vertical profiles of cloud fraction (for June, July, and August) averaged over six different regions covering the tropics, where the control run is shown by solid, NCWP by dashed, and NCW by dotted line. (a) Warm pool (120°E–180°E, ocean only); (b) Pacific Ocean east of 180°, ocean only; (c) South and Central America, land only; (d) Atlantic Ocean, ocean only; (e) Africa, land only; and (f) Indian Ocean, west of 120°E, ocean only. All regions extend from 25°N to 25°S.

Table 2a. Average CAPE in the Experiments (J/kg)

	WP Region	All Tropics
Control	201.3	−11.9
NCWP	403.9	72.3
NCW	615.7	302.7

All tropic extends from 20°S to 30°N.

20°N. There is only a modest (16%) drop within the WP area in the NCWP experiment (the drop east of WP is discussed below). There is no significant change in total tropical latent heating in NCWP and only a very small increase in NCW. Both experiments, however, show losses of latent heating in the WP region and gains in the eastern Pacific.

The changes to cloudiness and latent heating indicate that broad convection patterns closely follow patterns in circulation, as indicated in Figures 6–8. Stability differences seem to have played a role in determining the locations of new convection in NCW and in determining cloud altitudes, but the geographical distribution of convection does not respect the increases in stability directly (see Table 2), which were maximum in WP where cloudiness decreased the most. Thus in ECHAM3, convection seems to be controlled largely by atmospheric circulation rather than stability or surface temperature directly. It should be noted, however, that large fluctuations on synoptic spatial scales occurred in the experiments, including the appearance of new convection at the southern edge of WP and loss of convection east of WP. The synoptic scale changes were closely associated with wind-induced changes in surface evaporation. For example, the loss of convection east of WP in the NCWP simulation was apparently triggered by reduced surface evaporation caused by lower wind speeds associated with reduced low-level convergence into WP. Thus surface fluxes often seem to be able to determine the distribution of convection in unstable atmospheres on scales smaller than WP.

It is interesting to note that while total latent heat release decreased by only 16% in the WP region in NCWP, total cloud fraction decreased by 30%, indicating a drop in cloud lifetimes or formation efficiency. This drop strengthens an apparent positive feedback between CRF and cloud formation: CRF generates local ascent, which induces more cloud formation, which in turn can exert more heating. The sensitivity of cloud lifetime/formation efficiency may be partially due to the colder troposphere, which can increase precipitation rates by increasing the cloud ice fraction (model ice precipitation is far more efficient than liquid raindrop coalescence). It may also be associated with large-scale ascent, perhaps through its regulation of the upper tropospheric humidity and cloud evaporation rates.

Table 2b. Average Total Cloud Fraction in the Experiments

	WP Region	All Tropics
Control	0.593	0.467
NCWP	0.415	0.415
NCW	0.466	0.448

Total cloud fraction is the cloud fraction as seen from top-of-atmosphere and reflects the cloudiness at all of the levels and the degree of overlap.

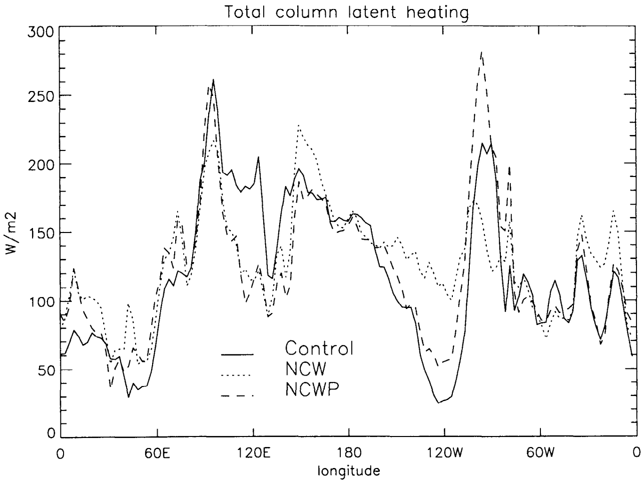

Figure 13. Equatorial variation of vertically averaged tropospheric latent heating in the control run, NCW, and NCWP (the Pacific covers roughly the middle third of the longitude axis). Values are averaged from 20°S to 20°N and include all net latent heating (condensation - evaporation of cloud/precipitation).

5.5. Effect on Humidity and the Surface Energy Budget

There is a great loss of atmospheric water vapor in regions losing large-scale ascent. Figure 14 shows the longitudinal distribution of tropical water vapor at 500 mbar in the control and experiment runs. In a relative-humidity conserving atmosphere the NCW specific humidity would be expected to drop by about 20% due to the temperature decrease at this altitude over most of the tropics and about 30% in the WP region (about 5 and 10%, respectively, for NCWP). This is roughly the decrease observed at 850 mbar (not shown), but at 500 mbar there is a significant redistribution of the vapor. In NCW the WP and eastern Indian Ocean regions lose about half of the their water vapor, the equatorial African and Central American atmospheres lose 10–20%, and part of the eastern Pacific atmosphere actually gains vapor. The results are similar at higher altitudes. The humidity changes in the NCWP experiment, where the temperature change is

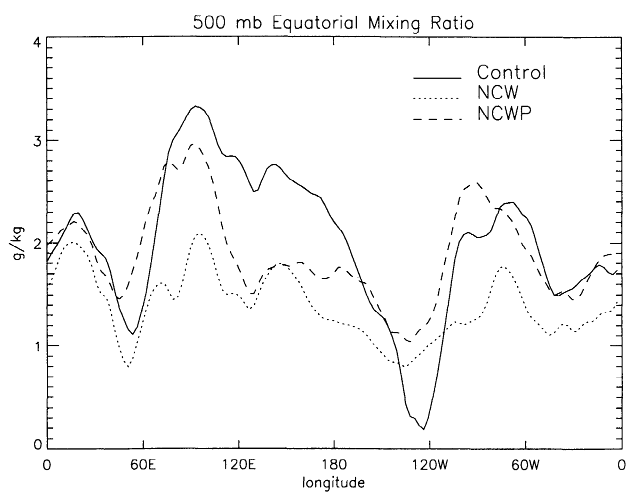

Figure 14. Equatorial section of mixing ratio at 500 mbar, averaged from 20°S to 20°N.

Table 3. Changes in the WP Surface and Atmosphere Energy Budget

	Total Column Change	Change in Atmosphere	Change in Ocean
Net shortwave	41	−3	44
Net longwave	−34	−25	−9
Evaporation	···	···	−8
Sensible heat	···	···	−2

Amounts shown are differences, in W/m^2, between the NCWP and the control run warm pool summer averages. Positive values indicate more heating, or less cooling, in the experiment run.

much smaller, show almost as much drying over the WP and more moistening over the eastern Pacific. Thus "clear-sky" longwave cooling could be affected by the changes in circulation. The actual changes in clear-sky cooling reflect not only the humidity change but also to a greater degree, the temperature change (see section 6).

It is important to examine the secondary effect of the temperature and humidity changes on the surface energy budget. In our experiments, however, these secondary effects turn out to be small compared to the direct changes in CRF. Table 3 shows that the changes in the surface and atmospheric energy budgets in the NCWP experiment closely match those expected from the cloud forcing directly; that is, the total column shortwave heating increase in the experiment occurs entirely within the ocean (with actual cooling in the atmosphere due to lost cloud shortwave absorption), while the total column longwave decrease is experienced primarily in the atmosphere. A moderate evaporation increase compliments the longwave change, which results from changes in convection and circulation (see section 6). The changes in surface sensible heat flux were less than 2 W/m^2.

5.6. Land Surface Response and the No Cloud (NC) Experiment

ECHAM3 predicts land temperatures using a five-layer soil model, in contrast to SST which is fixed. The land surface heat budget includes shortwave heating, net longwave heating, evaporative cooling, sensible heat flux, and ice/snow melt. Land temperatures changed by as much as 10°C in the experiments, with cooling on average but warming in many locations.

In the NC experiment, where clouds over land were transparent, we expected to see land warming in the tropics. Surprisingly, there was still a slight cooling on average, though less than in NCW. On land, therefore, the influence of local weather changes associated with remote oceanic cloud forcing was stronger than that of local cloud shading. The predominant cooling appears to be caused by increases in rainfall and surface evaporation over land. Since the NC and NCW simulations were similar in all other respects important to this study, we shall not discuss the NC experiment further.

5.7. Detailed Results, Warm Pool Averages

WP region averages of the different components of the column energy budget are listed in Table 4, together with averages of quantities which influence these. Figure 15 shows graphically the reorganization of the WP energy

Table 4. Averages of Selected Quantities Over the WP Region for July, From Tendency Runs

	Control	NCWP
Cloud radiative forcing, °C/d	0.428	0.001
Clear sky radiation (R), °C/d	−1.323	−1.267
Convective heating (CV), °C/d	1.231	1.258
Large-scale net condensation (LH), °C/d	0.268	0.000
Vertical advection (AD), °C/d	−.795	−.142
Horizontal advection, °C/d (M)	0.087	0.073
Surface sensible heat flux, °C/d (M)	0.042	0.056
Moisture convergence (MC), °C/d	0.494	0.209
ω, tropospheric average, -mbar/d	14.4	3.0
Evaporation (E), W/m^2	117	122
Evaporation (E), °C/d	1.005	1.049
2-m mixing ratio (q), g/kg	18.73	17.84
2-m windspeed (u), m/s	4.96	4.50
2-m cumulus drying, g kg^{-1}d^{-1}	5.56	5.98

Vertical velocity ω is defined positive upward.

budget in the NCWP experiment. Table 5 compares some experiment changes observed in this region with those averaged over a more zonally extended region, the "Walker" region, which represents the total tropical region affected by WP diabatic heating. Walker extends from 20°S to 30°N and from 80°E to 120°W. This reaches roughly to the eastward extremity of the Walker circulation according to observations and previous models [e.g., *Hartmann et al.*, 1984], with an additional westward branch of one-third this extent following the result of *Gill* [1980]. All quantities in the two tables are taken from the tendency runs. They will be discussed in the following section to help understand the circulation and cloudiness changes in the experiments.

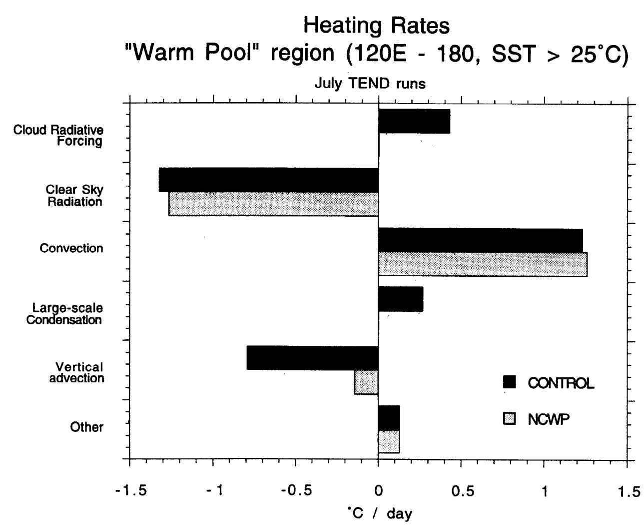

Figure 15. Heating rates from the July tendency runs in °C/d, control and NCWP. Convection is parameterized net cumulus heating; large-scale condensation is all other net condensation. The vertical advection term is cooling due to upward vertical motion against the subadiabatic lapse rate. "Other" is composed of advection by horizontal motions, sensible heat flux, gravity wave drag, and stratocumulus mixing (the latter two are of negligible magnitude).

Table 5. Average Experiment Differences NCWP-Control in WP and "Walker" Regions (Tendency Runs)

	Difference NCWP-Control	
	WP Region	"Walker" Region
Cloud radiative forcing (δCRF), W/m^2	−49.6	−14.5
Evaporation (δE), W/m^2	+5.1	+4.3
Clear-sky radiation (δR), W/m^2	+7.0	+5.3
ω, tropospheric average, -mbar/d	−11.4	−3.3
δE, (constant u) predicted, W/m^2	+15.9	+11.8
δE, (constant q) predicted, W/m^2	−7.9	−8.2

The bottom two rows indicate estimated partial changes in E from the influences of 2-m q and u individually. "Walker" is the region from 80°E to 120°W, 20°S to 30°N. Decreases in ω indicate decreases in ascent.

6. Discussion

The model CRF is only a third of the net latent heat release in the WP region. How can this relatively small factor have such a profound impact on the model circulation as seen in Figures 6–8? Consider the following points: (1) The net diabatic heating (sum of radiative cooling, convective and large-scale latent heating, and sensible heat flux) is about 0.6°C/d in the WP region (Table 4). (2) The CRF contribution to the net diabatic heating is 0.43°C/d (Table 4), or about 70% of the total. Thus it is plausible that CRF could have a large impact on circulation. We now explore how predictable the response is.

There are limited ways in which the model can respond to the loss of a significant heat source in a localized region such as WP. The model must balance atmospheric energy budget by adjusting the other significant processes in the budget until the shortfall has been compensated locally. These processes are clear-sky radiation, net condensation, surface sensible heat flux, and atmospheric heat advection. From Table 4 we find that for the NCWP experiment (1) the WP clear-sky radiative cooling only decreases enough to make up 5% of the lost CRF; (2) there is a loss of condensational heating, specifically large-scale heating, which increases the imbalance due to CRF by about 70%; (3) the horizontal heat advection and sensible heat flux terms remain small; and (4) an approximately fivefold reduction in vertical advection of sensible heat, associated with the vertical velocity change (Figure 11), compensates for the combined loss of CRF and large-scale condensational heating.

To try to gain some insight into the response, we will use conservation laws and fundamental behavioral properties of the tropical atmosphere to show that the possible atmospheric responses can be limited to a few types, and we will try to identify factors which decide which of these types will hold.

First, we write the energy budget explicitly for WP (or any fixed region) as

$$L + AD + R + M + \text{CRF} = 0 \quad (1)$$

where L is the total net latent heating by both convective and large-scale condensation; AD is the advective heating by vertical motion (negative in WP); R is the clear-sky radiative heating rate (also negative); and M is the other sources of heat, advection by horizontal motion and surface sensible heat flux. M is fairly small in WP and does not change in the experiments. All quantities are averages over the troposphere (100–1000 mbar), and their values are listed in Table 4.

Next, we consider the moisture budget,

$$L = E + MC. \quad (2)$$

Latent heat release L in a fixed region must be supplied by either local surface evaporation (E) or atmospheric moisture convergence (MC), where all quantities are heating equivalents (moisture fluxes multiplied by L_v/C_P). These values are also listed in Table 4.

Combining (1) and (2), applying the result to the control and experiment WP averages and subtracting, yields

$$\delta R + \delta E + \delta(AD + MC) = -\delta\text{CRF} \quad (3)$$

where all terms are differences, experiment minus control; δM has been neglected. The term in parentheses represents atmospheric advection of total moist energy, each of whose components AD and MC is determined mainly by vertical velocity in the tropics. Thus we have identified three exclusive mechanisms for compensating lost CRF: clear-sky radiative cooling, local surface evaporation, and moist energy advection by local ascent. The behavior of convection and large-scale condensation is implicit here, which is desirable because their behavior is difficult to explain or relate to other variables, even in the model. Evaporation and clear-sky cooling, on the other hand, are physical processes with clearly identifiable causes.

We note again that the magnitude of the moist energy export from WP in the control simulation is only 0.301°C/d (sum of AD, which is negative, and MC, which is positive, in Table 4). The δCRF term is larger than this, so without substantial changes to R and E a zeroth order change in ascent and thus large-scale circulation is required. We have shown that the model atmosphere's zonal eddies were significantly altered in the experiments, while the Hadley circulation and extratropical effects were modest. Next, we will examine this result in terms of processes which affect R and E locally underneath clouds and in the zonal average.

6.1. Analysis of the Zonal Eddy/Walker Circulation Response in No Cloud Over Western Pacific (NCWP)

Overturning eddies such as the Walker circulation are driven by differential heating between the ascending and descending branches of the eddy; this difference represents a "torque" which drives the eddy. Likewise, an eddy anomaly in an experiment simulation must be driven by differential heating anomalies. CRF represents a significant differential heat source since it appears only in cloudy regions, and its removal is thus a significant differential heating anomaly. Can the anomalies δR and δE be different enough between convective and nonconvective regions to exert a similar torque?

Clear-sky radiative cooling R is governed by the vertical profiles of temperature and humidity. In ECHAM3, natural variability of humidity in the tropics is found to be correlated in the upper and lower troposphere in such a way as to redistribute the heating vertically without significantly changing its column average. This is also true of the experiment-control changes. As a result, the column-averaged radiative cooling without clouds is determined by the temperature profile.

It is well known that time mean tropical temperatures above the boundary layer are approximately zonally uniform on isobars, due to the bouyancy driven adjustment [e.g., *Wallace*, 1992; *Holton*, 1992]. Approximate uniformity is reproduced by the model, and the temperature anomalies in the experiments also spread far zonally from the regions of lost heating. This leads to the conclusion that clear-sky cooling anomalies are diluted by zonal spreading, so that they cannot exert a significant torque to counteract that of δCRF. The mean temperature uniformity, incidentally, also plausibly accounts for the smallness of heat advection by horizontal motions on long temporal and spatial scales.

The δE was also small in WP and was approximately the same throughout the rest of the Pacific Ocean. We defer further consideration of the evaporation temporarily, except to note that the experiment change was small enough that even if it had been limited to WP, it would have produced an insignificant torque compared to that of δCRF. Thus with no significant differential heating responses in the zonal direction, it follows that the large zonal readjustments in the experiments were inevitable.

6.2. Zonal Mean Response

We have considered so far the response of zonal eddies to CRF. The response of the zonal mean in which these eddies are embedded, which has relevance to the Hadley circulation and extratropical response, is also of interest. It is of particular importance to recognize the impact of zonal heating inhomogeneities on the zonal mean state, since much of our understanding of the planetary circulation and climate comes from zonally symmetric models. While temperature changes spread widely in the zonal direction, they do not spread outside of the tropics easily. This is because meridional gradients can be balanced by steady geostrophic flow and by dissipative mechanisms such as turbulence generated by baroclinic instability. We will not discuss these mechanisms but shall merely suppose that some unspecified dynamical relationship exists between a zonal mean temperature anomaly and the moist-energy advection anomaly to other latitudes.

The zonal spreading of δR and δE away from the regions of δCRF means that the zonal mean budget is balanced by a more equitable combination of the three available processes on the left-hand side of (3) than the mainly $\delta(AD+MC)$ adjustment which occurred in WP alone, as shown by the Walker averages in Table 5. In each of our experiments, δR approximately equalled $\delta(AD+MC)$. Since δR is proportional to the zonal average temperature anomaly, its relationship to the energy advection $\delta(AD+MC)$ is determined by dry dynamics, addressed, for example, by *Held and Hou* [1980]. We will instead examine the response δE to investigate the sensitivity of the zonally averaged responses to model physics.

Surface evaporation is represented in the model by a standard bulk formula,

$$E = c_E u(q_S - q_a)$$

where u is a near-surface wind speed, q_S is the saturation mixing ratio at the surface, q_a is the near-surface mixing ratio, and c_E is a dimensional coefficient which depends on stability near the surface and wind speed. A linearized version of this equation has been used to estimate the partial changes to evaporation $(\partial E/\partial u)\delta u$ and $(\partial E/\partial q_a)\delta q_a$, resulting from surface air changes averaged over the Walker region. These changes, shown in Table 5, indicate that while the net δE was small, these compensating partial changes were individually comparable to δCRF. The drying δq_a was apparently due to an increase in cumulus drying, also shown in the table. Cumulus downdrafts are included in ECHAM3 and play an important role in modifying the boundary layer [*Zipser*, 1969; *Betts*, 1976].

One possible interpretation of the u and q changes is in terms of two feedbacks to the zonal mean energy budget involving evaporation: (1) zonal-eddy/evaporation feedback, a positive feedback whereby zonal eddies driven by condensation and CRF increase the surface wind speed and evaporation; (2) lapse-rate/evaporation feedback, a negative feedback whereby CRF increases atmospheric stability, decreasing vertical mixing of water out of the boundary layer, increasing surface moisture, and suppressing evaporation.

Each of these feedbacks could involve the evaporation throughout the eddy anomaly, not just where the CRF changes, and thus constitute a feedback to zonally averaged condensation. There may be other relevant controls on the mean surface wind speed and humidity, particularly the requirement of boundary layer moisture balance in regions of steady subsidence, but the above feedbacks are at least consistent with the results of the present experiments.

If these two feedbacks effectively accounted for the simulated changes, they were nearly equal and opposite. This would mean that the small evaporation response may not be robust, since the two feedbacks depend on completely different physical mechanisms. While the wind feedback depends on resolved motions, the lapse rate feedback depends on vertical transports by unresolved motions, which are poorly understood and crudely represented in GCMs. For instance, an alternate method of handling cumulus convection in numerical models would be to assume that it maintains a strict upper limit on CAPE [e.g., *Emanuel*, 1991]. With this assumption the surface moisture feedback could be about twice as strong as with ECHAM3 cumulus physics, since the NCWP simulated δq_a in the Walker region was only half what would have been required to neutralize CAPE changes. At the other extreme the neglect of direct, explicit communication between the boundary layer and the upper troposphere could make this feedback significantly weaker. One may speculate that differences in the strength of this feedback account for the differences in Hadley circulation response between the present NCW experiment (~25% reduction), SS (<20% reduction), and RHDC (~50% reduction) [see also *Miller et al.*, 1992]. However, many other differences between the studies preclude any firm conclusions about this.

7. Conclusion

We have shown using a recent version of the ECHAM3 AGCM that cloud radiative interactions can have a significant influence on global circulation patterns. The AGCM used in this study has been shown to simulate observed top-of-atmosphere flux data collected by ERBE successfully. Other studies [*Slingo and Slingo*, 1988; *Randall et al.*, 1989] have already demonstrated model sensitivity to cloud radiation. We have built on these studies by using a model whose radiation results can be compared with observations, by investigating carefully the sensitivity of zonal circulations to CRF, and by attempting to establish the key mechanisms which determine the character and magnitude of the response.

The primary effect of CRF in the atmosphere is to warm the troposphere, particularly the upper troposphere, and to cool the surface. The net column (ocean plus atmosphere) effect is small, but the redistribution of energy from ocean to atmosphere gives CRF over oceans a large impact on the atmospheric circulation and the oceanic heat budget. Over land, the effect seems to be limited to local surface temperature adjustments. The magnitude of the tropospheric heating due to tropical high cloud is small compared to the largest terms in the budget, latent heating and radiative cooling. However, the atmospheric response to CRF is dictated not by how it compares to arbitrarily chosen terms in the budget but instead by how the heating compares with the atmospheric moist energy transport, which is small in the simulated atmosphere.

The simulated atmosphere in the control run had strong zonal circulations in the tropics. The area of greatest ascent included Indonesia, southern Asia, and the western Pacific. The removal of radiative forcing of tropical high clouds leads to zeroth order changes in the tropical circulation, as indicated by the upper tropospheric divergence and vertical velocity. In the NCW simulation, where high-cloud CRF was removed over tropical oceans, about 25% of the Hadley circulation and most of the Walker circulation disappeared. The NCWP simulation, where only western Pacific CRF was removed, lost only about 10% of the Hadley circulation but experienced a significant rearrangement of the tropical zonal circulation, with warm-pool ascent falling from well above to below the tropical average. Previous studies have found CRF to be an important factor in the maintenance of the Hadley circulation; we find it to be even more important for the Walker circulation.

Atmospheric CRF is a strong differential heat source which has the capability to drive zonal eddies comparable to those simulated in the control atmosphere. Surface fluxes and clear-sky cooling are the only two other significant sources of moist energy to the atmospheric column besides vertical advection, but their anomalies are apparently confined to long zonal scales, preventing them from exerting any comparable influence of their own on zonal eddy anomalies in the experiments. Zonally averaged temperature and circulation responses to CRF are, however, moderated by nontrivial clear-sky cooling and evaporation anomalies, the latter of which may rely on a sensitive balance between competing feedbacks involving different physical mechanisms. This means that uncertainties as to the correct parameterizations of cumulus convection and evaporation, which are both controversial at the time of this writing, may project strongly onto the response of the Hadley and extratropical circulations.

Any process which affects the circulation will similarly affect precipitation. Significant redistributions of condensation occurred in the experiments which generally matched the redistributions of large-scale ascent. Patterns of water vapor and cloud cover change also matched the changes in ascent. In areas of high SST where CRF was removed, local cloud cover dropped substantially, indicating a positive local feedback between cloud radiative heating and cloud formation. This feedback may be enhanced by local temperature and humidity changes, which shorten the lifetimes of clouds in the experiments. In the NCW experiment, cloud cover increased over colder oceans but decreased over warm oceans, as stability apparently became less important in determining the distribution of convection. Net tropical cloudiness changes in both experiments were small compared to zonal redistributions, but there was a notable loss of low cloud overall in NCW, probably due to the increase in instability which favors high-cloud formation. In the WP region the parameterized convective heating stayed about the same in the NCWP experiment as in control, but this represents a fortuitous cancelation of the effects of increased instability and decreased moisture supply. The total condensation anomalies are highly correlated with upper level divergence anomalies.

The primary results of this study are that a seemingly moderate localized tropical atmospheric heat source is capable of widespread influence on the circulation and that CRF is such a source. The opposite result, which might have occurred, for instance, if evaporative feedbacks had been strong enough to negate atmospheric heat sources, would have meant that the circulation is controlled tightly by SST. Diabatic heat sources placed in the atmosphere would affect convection but would not affect large-scale circulation until they did so indirectly by warming SST. Heating dipoles such as CRF would, in this scenario, significantly affect neither circulation nor SST, only local evaporation and rainfall. Our result indicates on the contrary that conditional heating in the atmosphere (including cloud radiative effects) plays a sufficiently important role that it must be handled carefully to obtain realistic simulations.

Acknowledgments. Thanks to the Max Planck Institute without whose cooperation this project would not have been possible and to Ulrich Schlese for his personal assistance. Thanks also to the reviewers for their generous and helpful comments. This study was supported by Department of Energy grant DOE DEFG 0391 ER 61198 in conjunction with the ARM (Atmospheric Radiation Measurement) Program.

References

Betts, A. K., The thermodynamic transformation of the tropical sub-cloud layer by precipitation and downdrafts, *J. Atmos. Sci.*, *33*, 1008–1020, 1976.

Cess, R. D., et al., Interpretation of cloud-climate feedback as produced by 14 atmospheric general circulation models, *Science*, *245*, 513–516, 1989.

Emanuel, K. A., A scheme for representing cumulus convection in large-scale models, *J. Atm. Sci. 48*, 2313–2335, 1991.

Gill, A. E., Some simple solutions for heat-induced tropical circulation, Q. J. R. Meteorol. Soc., *106*, 447–462, 1980.

Hallberg, R., and A. K. Inamdar, Observations of seasonal variations in atmospheric greenhouse trapping and its enhancement at high sea surface temperatures, *J. Clim.*, *6*, 920–931, 1993.

Harrison, E. F., P. Minnis, B. R. Barkstrom, V. Ramanathan, R. D. Cess, and G. G. Gibson, Seasonal variation on cloud radiative forcing derived from the Earth Radiation Budget Experiment, *J. Geophys. Res.*, *95*, 18,687–18,703, 1990.

Hartmann, D. L., H. H. Hendon, and R. A. Houze Jr., Some implications of the mesoscale circulations in tropical cloud clusters for large-scale dynamics and climate, *J. Atmos. Sci.*, *41*, 113–119, 1984.

Held, I. M., and A. Y. Hou, Nonlinear axially symmetric circulations in a nearly inviscid atmosphere, *J. Atmos. Sci.*, *37*, 515–533, 1980.

Hoerling, M. P., M. L. Blackmon, and M. Ting, Simulating the atmospheric response to the 1985–87 El Nino cycle, *J. Clim.*, *5*, 669–682, 1992.

Holton, J. R., *An Introduction to Dynamic Meteorology*, Academic, San Diego, Calif., 1992.

Hoskins, B. J., and D. J. Karoly, The steady linear response of a spherical atmosphere to thermal and orographic forcing, *J. Atmos. Sci.*, *38*, 1179–1196, 1981.

Houze, R. A., Cloud clusters and large-scale vertical motions in the tropics, *J. Meteorol. Soc. Jpn.*, *60*, 396–410, 1982.

Johnson, D. R., M. Yanai, and T. K. Schaack, Global and regional distributions of atmospheric heat sources and sinks during the GWE, in *Monsoon Meterology*, edited by C. P. Chang and T. N. Krishnamurti, Oxford at the Clarendon Press, London, 1987.

Lorenz, E. N., Available potential energy and the maintenance of the general circulation, *Tellus*, *7*, 157–167, 1955.

Miller, M. J., A. C. M. Beljaars, and T. N. Palmer, The sensitivity of the ECMWF model to the parameterization of evaporation from the tropical oceans, *J. Clim.*, *5*, 418–434, 1992.

Ramanathan, V., and W. Collins, Thermodynamic regulation of ocean warming by cirrus clouds deduced from observations of the 1987 El Niño, *Nature*, *351*, 27–32, 1991.

Ramanathan, V., E. J. Pitcher, R. C. Malone, and M. L. Blackmon, The response of a spectral general circulation model to refinements in radiative processes, *J. Atmos. Sci.*, *40*, 605–630, 1983.

Ramaswamy, V., and V. Ramanathan, Solar absorption by cirrus clouds and the maintenance of the tropical upper troposphere thermal structure, *J. Atmos. Sci.*, *46*, 2293–2310, 1989.

Randall, D. A., Harshvardhan, D. A. Dazlich, and T. G. Corsetti, Interactions among radiation, convection, and large-scale dynamics in a general circulation model, *J. Atmos. Sci.*, *46*, 1943–1970, 1989.

Roeckner, E., et al., Simulation of the present-day climate with the ECHAM model: Impact of model physics and resolution, *Tech. Rep. 93*, 171 pp., Max-Planck-Inst. für Meteorol., Hamburg, Germany, 1992.

Sardeshmukh, P. D., and B. J. Hoskins, Vorticity balances in the tropics during the 1982–83 El Niño-Southern Oscillation event, *Q. J. R. Meterol. Soc.*, *111*, 261–278, 1985.

Slingo, A., and J. M. Slingo, The response of a general circulation model to cloud longwave radiative forcing, I, Introduction and initial experiments, *Q. J. R. Meterol. Soc.*, *114*, 1027–1062, 1988.

Stephens, G. L., and P. J. Webster, Sensitivity of radiative forcing to variable cloud and moisture, *J. Atmos. Sci*, *36*, 1542–1556, 1979.

Tiedtke, M., A comprehensive mass flux scheme for cumulus parameterization in large-scale models, *Mon. Weather Rev.*, *117*, 1779–1800, 1989.

Waliser, D. E., N. E. Graham, and C. Gautier, Comparison of the highly reflective cloud and outgoing longwave radiation data sets for use in estimating deep tropical convection, *J. Clim.*, *6*, 331–353, 1993.

Wallace, J. M., Effect of deep convection on the regulation of tropical sea surface temperature, *Nature*, *357*, 230–231, 1992.

Williams, E., and N. Renno, An analysis of the conditional instability of the tropical atmosphere, *Mon. Weather Rev.*, *121*, 21–36, 1993.

Zipser, E. J., The role of organized unsaturated convective downdrafts in the structure and rapid decay of an equatorial disturbance, *J. Appl. Meteorol.*, *8*, 799–814, 1969.

T. P. Barnett, V. Ramanathan, S. C. Sherwood, and M. K. Tyree, Scripps Institution of Oceanography, University of California at San Diego, La Jolla, CA 92093-0239.

E. Roeckner, Max-Planck-Institut für Meteorologie, Hamburg, Germany.

(Received June 16, 1993; revised May 7, 1994;
accepted June 17, 1994.)